Arabian Journal of Chemistry (2023) **16**, 104469

King Saud University

Arabian Journal of Chemistry

www.ksu.edu.sa
www.sciencedirect.com

ORIGINAL ARTICLE

Theoretical and experimental study of new deep eutectic solvents for extraction of perfluorinated iodoalkanes

Chen Fan [*,1], **Yingyi Han** [1], **Yaqi Yin, Yuwei Shan, Xueli Cao**

Beijing Advanced Innovation Center for Food Nutrition and Human Health, Beijing Technology and Business University, Beijing 100048, China

Received 25 July 2022; accepted 24 November 2022
Available online 1 December 2022

KEYWORDS

Perfluorinated iodoalkane;
Deep eutectic solvent;
Partitioning behavior;
Structure-property-performance relationship;
Synergism mechanism

Abstract There is a lack of attention and reporting in aspects of the neutral/nonionic perfluoroalkyl substances (PFASs) and corresponding treatment mechanisms. Herein, new function-oriented deep eutectic solvents (DESs) with pyridine moiety were designed for perfluorinated iodoalkanes extraction from the oil phase. The effect of hydrogen bond acceptor (HBA) functional groups on the effectiveness of targets retrieval was investigated. Moreover, different structural, quantum-chemical, solvatochromic, and statistical thermodynamics parameters were conducted, calculated, and correlated to the distribution coefficients of the studied DESs. Results showed that functional groups of HBAs significantly affected the extraction effectiveness of eutectic mixtures. The pyridine ring-based DESs with the C═O group possessed the highest extraction efficiencies among the studied groups. To some extent, the extraction performances of the DES were substantially affected by the electrostatic potential extrema of the donor halogen atom and pyridine analogues. For targets with relatively short alkyl chain length, the topological indices had a positive relationship with the treatment efficacy of the DESs, and the quantum-chemical parameters of these solvents had a strong negative relationship with them. For targets with long alkyl chain length, the solvatochromic parameters of DES had a great influence on the distribution coefficients and also on the selectivity of these solvents. Furthermore, the halogen and hydrogen bonds presented cooperativity, clarifying via quantum-chemistry calculations. The synergism mechanism between them is

* Corresponding author at: NO. 11 Fucheng Road, Beijing Technology and Business University, Beijing 100048, China.
E-mail address: fanchen@btbu.edu.cn (C. Fan).
[1] Chen Fan and Yingyi Han contributed equally to this work.

Peer review under responsibility of King Saud University.

Production and hosting by Elsevier

https://doi.org/10.1016/j.arabjc.2022.104469

beneficial to the extraction of perfluorinated iodoalkanes. Besides shedding light on the structure–property-performance relationships of the DESs, these findings also provided novel insights into the directional design and selection of DESs.

1. Introduction

Perfluoroalkyl substances (PFASs) are a large class of man-made chemicals. Thousands of distinct PFASs were widely used in consumer products and industrial processes, where the use is not readily public or available (Gaines, 2022). They generally consist of a carbon backbone replaced by fluorines and at least one functional group, such as a sulfonic acid, carboxylic acid, amine, iodine, or other. Diverse PFASs belong to the subclass of "precursors" that can be transformed into highly persistent PFASs, and may be more toxic or bioaccumulative than their final products (McDonough et al., 2022). Perfluorinated iodoalkanes or polyfluorinated iodine alkanes (PFIs) have been reported to have the potential to be converted into related perfluoroalkyl carboxylates (Ruan et al., 2010). Several PFI homologues had dramatic increases in production volumes per year, and are thus included on the high production volume (HPV) list. The U.S. Environmental Protection Agency PFAS Action Plan applied systematic evidence map (SEM) approaches to characterize the evidence base for over 150 PFASs and provide a high-level summary of identified PFASs (Carlson et al., 2022). The PFI (perfluoro-1-iodohexane) could be found in the list. In contrast to the many PFASs with merely-one assigned use, this kind of compound has many uses or was employed more frequently, especially in oil productions, such as oil additives, cutting or drawing oil, surface active agents in oil drilling, and so on (Gaines, 2022; Glüge et al., 2020). A plenty of materials and solvents, including ionic liquids, were developed for the treatment and removal of PFASs, and most of them focused on the ionizable subclasses (Grabda et al., 2022). There is a lack of attention and reporting in aspects of the neutral/nonionic PFASs and corresponding mechanisms.

Novel green solvents called deep eutectic solvents (DESs) have recently attracted considerable attention from the scientific community in various fields. They can be prepared by two components, one as a hydrogen bond donor (HBD), and another as a hydrogen bond acceptor (HBA) (Abbott et al., 2021). Researchers discovered that the obtained eutectic mixture had a significantly lower melting point than that of its original ingredients. The liquid structure of DES is directed by a combination of inter- and intra-molecular interactions, including hydrogen bonding, coulomb forces, van der Waals interactions, apolar-polar segregation, dispersion forces, and electrostatics (Bryant et al., 2022). Their unique attributes, such as simple preparation, high atom economy, low cost, non-flammability, and less toxicity, are the primary advantages, which make them have broad application prospects in separation (Florindo et al., 2017, Makoś et al., 2020), gas capture (Zubeir et al., 2018), biomass pretreatment (Satlewal et al., 2018), catalysis (Yu et al., 2022), solar cells (Boldrini et al., 2018), and so on. The physicochemical properties and unique performance of DESs are finely tuned depending on their starting materials via different combinations and proportions of HBA and HBD. The current development of novel DESs is mostly driven by applications, while rational DES design can be achieved only once structure-performance relationships are established (van den Bruinhorst et al., 2021). Moreover, their physicochemical properties database is urgently needed due to the fact that physicochemical properties data will offer sufficient information for the structure–property-performance relationship (Zainal-Abidin et al., 2021). The molecular approach, such as quantitative structure–property relationship (QSPR) as a robust method, can develop a mathematical relationship between the physicochemical properties and the molecular features of the analyzed structures (Balali et al., 2021). Additionally, molecular simulations and modeling can also be helpful and beneficial in elucidating the basics and fundamental performance of these eutectic solvents.

Electronegative atoms, such as iodines, can have electropositive potential regions within the electron density. This electropositive area is called the σ-hole, and it provides an attraction region for the specific molecule containing an atom with a lone pair electrons. The σ-hole enables iodine to behave analogously to the way electropositive hydrogen does in hydrogen bonding (Fan et al., 2009). As a result of the great electron-withdrawing power of fluorine atoms on the alkane backbone, iodo-perfluoroalkanes are viable to contain a particularly strong σ-hole on the lone iodine, and the hydrogen bonding between these substances and pyridines is comparable to the hydrogen bonding between pyridines and alcohols (von der Heiden et al., 2020). Inspired by this, the new function-oriented DESs with the pyridine moiety can be designed for perfluorinated iodoalkanes retrieval from the oil phase.

In this work, we synthesized and characterized a series of eutectic mixtures composed of 14 types of pyridine analogues and glycolic acid (as a common HBD) for investigating the effect of HBA functional groups on the effectiveness of the neutral/nonionic perfluoroalkyl substances extraction from oil phase. This was evaluated by the selective liquid–liquid partitioning behaviour of perfluorinated iodoalkanes. Most importantly, different structural, quantum-chemical, solvatochromic, and statistical thermodynamics parameters, including connectivity index, polarity, hydrogen bond acidity, hydrogen bond basicity, H_int, H_MF, H_vdW, infinite dilution activity coefficient, total energy, and the lowest unoccupied and highest occupied molecular orbital energies of the solvents, were conducted, calculated, and correlated to the distribution coefficients of the studied DESs toward perfluorinated iodoalkanes, with an attempt to establish structure–property-performance relationships and to elucidate the corresponding mechanism of pyridine ring-based eutectic system. As far as we know, this is the first study to demonstrate the relationship between the extraction efficiency of the designed DESs toward perfluorinated iodoalkanes and their structural features/physicochemical properties through a combination of experimental and theoretical studies.

2. Materials and methods

2.1. Chemicals and reagents

Pyridine hydrochloride (purity: 98 %), 2, 2′-bipyridyl (99 %), 2-aminopyridine (99 %), 3-aminopyridine (99 %), 4-aminopyridine (98 %), 2-hydroxypyridine (97 %), 3-hydroxypyridine (99 %), 4-hydroxypyridine (97 %), methyl nicotinate (99 %), nicotinohydrazide (97 %), nicotinamide (99 %), nicotinic acid (99 %), 2-picolinic acid (99 %), 2-pyridinemethanol (98 %), glycolic acid (98 %), phenol (≥99.5 %), p-cresol (99 %), p-nitrophenol (>99.0 %), 4-methoxyphenol (99 %), glycolic acid (98 %) were bought from Shanghai Macklin Biochemical Technology Co., ltd. Perfluorinated iodoalkane standards (>99.0 %), including perfluorobutyl iodide (PFBI, C4F9I), perfluorohexyl iodide (PFHxI, C6F13I), perfluorooctyl iodide (PFOI, C8F17I), perfluorodecyl iodide (PFDeI, C10F21I), and perfluorododecyl iodide

(PFDoI, C12F25I) were obtained from Sigma-Aldrich (St. Louis, MO). Fatty acids standards (>99.0 %), including butyric acid (C4H8O2), hexanoic acid (C6H12O2), octanoic acid (C8H16O2), decanoic acid (C10H20O2), and dodecanoic acid (C12H24O2), were purchased from Macklin Biochemical Technology. The dyes for solvatochromic parameters, including 4-nitroanisole, 4-nitroaniline, and Nile red, were obtained from Tianjin Heowns Biochemical Technology Co., ltd. Acetonitrile and ammonium acetate employed in instrumental analysis were of mass grade (>99.99 %, Fisher, USA). *N*-hexane was bought from Tianjin Fuchen Chemical Reagent Co., ltd. and was of analytical grade.

2.2. Preparation and characterization of eutectic solvent systems

Eutectic solvent systems were prepared by mixing the above sources at different molar ratios and at 343.15 K for 15–30 min. For obtaining the liquid eutectic system at room temperature, the HBD:HBA molar ratios of these mixtures were kept at 5:1 in the next characterization and extraction processes. All of these systems and their starting materials were measured by Attenuated Total Reflection Fourier transformed Infrared Spectroscopy (ATR-FTIR, IRTracer-100, SHIMADAU, Japan). Their spectra for functional groups were recorded in the range of 4000–400 cm^{-1} with 50 scans at 298.15 K. The melting point for the DESs was determined by differential scanning calorimetry (DSC, TA Instruments Q2000, USA) in a temperature range of 183.15–573.15 K with a 10 K min^{-1} heating/cooling rate. The solid–liquid phase equilibria can be described by Schröder equation according to the published works (Fan et al., 2022). The solvatochromic parameters of these DES systems were carried out according to the published protocols (Kundu et al., 2020; Jessop et al., 2012). The parameters of some solvents cannot be obtained because of the precipitation phenomenon when adding dyes. The viscosities of the DES systems were measured at 298.15 K using a NDJ-8S digital rotational viscometer (viscosity 2 %).

2.3. Liquid–liquid equilibrium experiments

An *n*-hexane solution with a low concentration of five perfluorinated iodoalkanes and fatty acids (100 mg/L) was used as the model for the oil phase to study the extraction ability of the proposed DESs. For the liquid–liquid equilibrium experiment, 3 mL of model solution was added into a 10 mL screw flask, and different DES (equal volume) with a HBD:HBA molar ratio of 5:1 was added at the same time. The flask was sealed and placed in the metal bath at a constant temperature of 298.15 K. The mixture was stirred at 2000 rpm for 1 h and then settled for 1 h to ensure equilibrium. Finally, the DES phase and the *n*-hexane phase were sampled and analyzed. Distribution coefficients (β) = mass fractions of target in DES/mass fractions of target in *n*-hexane. Selectivity (S) = $\beta_{\text{perfluorinated iodoalkane}}/\beta_{\text{fatty acid}}$.

2.4. Analysis of perfluorinated iodoalkanes and fatty acids

Quadrupole Time-of-Flight Mass Spectrometer (QTOF-MS) (Xevo G2-XS, Waters Co., ltd., Wilmslow, UK) equipped with electrospray ionization (ESI) interface was performed in the negative-ion and selective ion monitoring mode. Capillary voltage: 3.0 kV. Source temperature: 373.15 K. Desolvation temperature: 823.15 K. Five fatty acids were separated by ultra-performance liquid chromatography (Waters Co., ltd., UK). Column: ACQUITY® BEH C18 column (2.1 × 50 mm, 1.7 μm). Column temperature: 303.15 K. Flow rate: 0.5 mL min^{-1}. Injection volume: 1 μL. The mobile phase was methanol (A) and 2 mmol/L ammonium acetate aqueous solution (B). Gradient elution: 90 % B for 0.5 min, from 90 % to 0 % in 15 min, a final isocratic 0 % for 1.0 min, from 0 % to 90 % in 0.1 min, and 90 % for 3 min to allow whole system re-equilibration. Quantification was performed by standard curve analysis by plotting the response of the respective molecular ions (butyric acid: 87.0972; hexanoic acid: 115.1503; octanoic acid: 143.2035; decanoic acid: 171.2567; dodecanoic acid: 199.3098).

The gas chromatography (GC) instrument (Agilent 7890B) was equipped with MassHunter software and coupled with a triple quadrupole mass spectrometer (Agilent 7000C). GC separation was implemented on a HP-5MS capillary column (30 m × 0.25 mm × 0.25 μm; Agilent). The injector temperature and injection volume were set to 543.15 K and 1 μL, respectively. The flow rate of carrier gas (helium) was 1.0 mL min^{-1}. Initially, the oven temperature program was kept at 308.15 K for 6 min. Then, the temperature was increased to 403.15 K at 5 K min^{-1}. The mass ion source temperature was 523.15 K and the interface temperature was 553.15 K. Electron impact (EI) ionization mode and selective ion monitoring mode were used. Quantification was performed by standard curve analysis by plotting the response of the respective molecular ions (PFBI: 345.9; PFHxI: 318.9; PFOI: 226.9; PFDeI: 519.0; PFDoI: 619.0).

2.5. Computational details

Geometries and energies of DES complexes, their components, and perfluorinated iodoalkanes were fully optimized at the M06-2X/aug-cc-pVTZ level with Grimme's DFT-D3 empirical dispersion correction using Tmolex (version 21.0.0), except for iodine, for which the aug-cc-pVTZ-PP basis set was used. Basis set superposition errors (BSSE) were not computed since it has been shown that uncorrected aug-cc-pVTZ energy lies between the corrected and uncorrected aug-cc-pVQZ energy (Alkorta et al., 2010). The thermodynamic properties, total mean interaction energies (H_int), misfit interaction energies (H_MF), van der Waals interaction energies (H_vdW), and infinite dilution activity coefficient were calculated by the software COSMOtherm (version 21.0.0). The topological indices (Connectivity index) of different solvents were conducted with MathChem (Vasilyev, 2014). The related electrostatic potential and extreme points in the global surface were done by Multiwfn package 3.7 (Lu and Chen, 2012). The properties of the considered DESs were studied at the short-range hydrogen bonding by analyzing minimal HBA:HBD and HBD:HBD clusters at a 1:1 ratio (Gutiérrez et al., 2022). For convenient and direct investigation of hydrogen and halogen bonds among HBA, HBD, and targets, corresponding interaction energies calculations were done in the molar ratios of 1:1:1 during density functional theory analysis.

Dimer (hydrogen-bond) is denoted by A-B, and dimer (halogen-bond) is denoted by B-C; A-B-C represents trimer. Here, A, B, and C are glycolic acid, pyridines, and perfluori-

nated iodoalkanes, respectively. The interaction energies of the hydrogen bond and halogen bond in dimers were calculated using the equations $\Delta E_{AB} = E_{AB} - (EA + EB)$ and $\Delta E_{BC} = -E_{BC} - (EB + EC)$, respectively. The interaction energies of hydrogen bond and halogen bond in trimers were calculated using the equations $\Delta E_{AB}' = E_{ABC} - (EA + E_{BC})$ and $\Delta E_{BC}' = E_{ABC} - (EC + E_{AB})$, respectively. E_{ABC} is the total energy of the ternary system. EA, E_{BC}, EC, and E_{AB} are the energies of the binary and monomeric systems. The interaction energy of the ternary system was obtained by the equation $\Delta E_{ABC} = -E_{ABC} - (EA + EB + EC)$. The cooperative energy (E_{coop}) was calculated by the equation $E_{coop} = \Delta E_{ABC} - \Delta E_{AB} - \Delta E_{BC} - \Delta E_{AC}$. ΔE_{AC} is the interaction energy between A and C in the trimer (Zhao et al., 2011).

3. Results and discussion

3.1. Preparation and characterization

Fourteen pyridine-based and four phenol-based derivatives (for comparison) were chosen as HBAs, and glycolic acid was employed as an HBD (Fig. 1). The melting properties of all the DES components are given in Table 1. We aimed to develop hydrophilic and oil-stable eutectic systems. According to the previous literature, the chemical nature of DES components determines the hydrophilicity or hydrophobicity of the final product (Taghizadeh, et al., 2021). The hydrophilicity of DES was relatively high, where higher portions of the hydrophilic component resulted in lower oil solubility (Lee, et al., 2019). The logP values of these starting materials were low, thus the mutual solubility of the obtained eutectic systems and *n*-hexane was expected to be low. The conductor-like screening model for real solvents (COSMO-RS) was used to

Table 1 Compounds used for the preparation of deep eutectic solvents and their melting properties.

Compound	CAS	T_m/K	$\Delta_m h$/kJ·mol^{-1}
Pyridine hydrochloride	628-13-7	419.15	14.630
2, 2′-Bipyridyl	366-18-7	345.15	20.014
2-Aminopyridine	504-29-0	331.15	13.0819
3-Aminopyridine	462-08-8	337.65	13.0819
4-Aminopyridine	504-24-5	434.15	13.0819
2-Hydroxypyridine	142-08-5	380.95	14.0569
3-Hydroxypyridine	109-00-2	403.15	14.0569
4-Hydroxypyridine	626-64-2	422.95	14.0569
Methyl nicotinate	93-60-7	315.65	17.434
Nicotinohydrazide	553-53-7	436.15	22.280
Nicotinamide	98-92-0	403.15	17.271
Nicotinic acid	59-67-6	509.75	20.618
2-Picolinic acid	98-98-6	409.65	20.618
2-Pyridinemethanol	586-98-1	278.15	14.5629
Glycolic acid	79-14-1	348.15	15.167
Phenol	108-95-2	314.05	11.509
p-Cresol	106-44-5	308.65	13.710
p-Nitrophenol	100-02-7	387.15	22.481
4-Methoxyphenol	150-76-5	330.15	14.898

T_m: melting (fusion) point; $\Delta_m h$: Enthalpy of fusion.

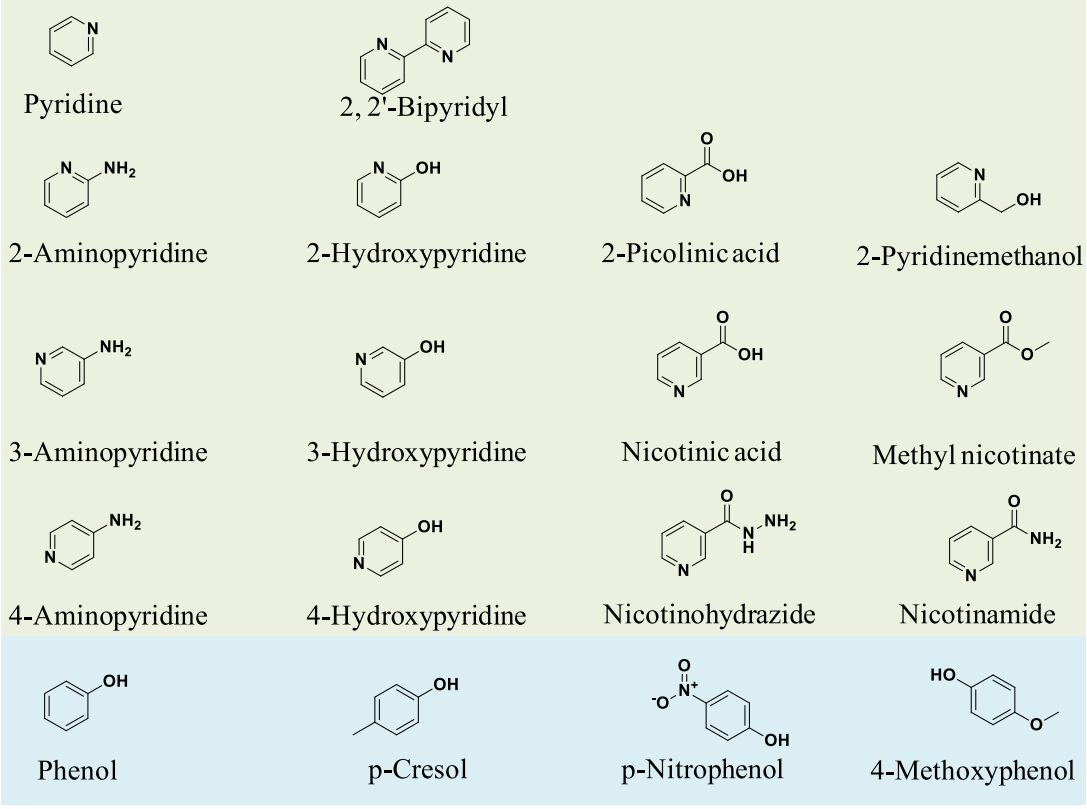

Fig. 1 The structures of compounds used for the preparation of deep eutectic solvents.

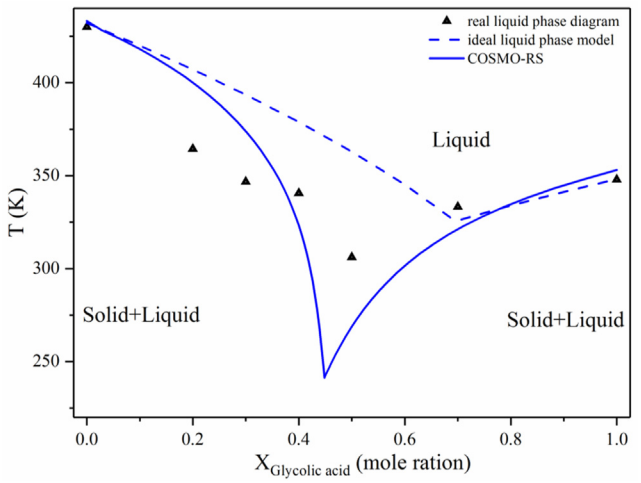

Fig. 2 Experimental solid–liquid equilibrium phase diagram of the glycolic acid-4-aminopyridine system (▲) measured by the differential scanning calorimeter, and the predictions by COSMO-RS (full line), along with the ideal liquidus line (dashed line).

calculate the melting points of different solvent systems for the estimation of the solid–liquid equilibrium phase conditions (Fan et al., 2021a). The predicted and measured phase diagrams are shown in Fig. 2, along with the ideal liquidus curve. The mixtures of glycolic acid and 4-aminopyridine present a sharp decrease in the melting point, compared with the initial substances. In the experimental phase diagram, the lowest temperature depression can be observed for this system with a glycolic acid:4-aminopyridine molar ratio of 1:1, while in the predicted and ideal diagrams it occurs at molar ratios of 1:1.2 and 2.3:1, respectively. The non-ideal phase behavior of the eutectic system can be explained by the excess entropy and enthalpy (Shishov et al., 2022). Moreover, the eutectic point temperatures of the solvent system present strong negative deviations from ideality, which is consistent with the current definition of DES. The diagrams of other systems are in Fig. S1.

The FTIR spectra for different solvent systems and their pure sources are presented in Fig. 3. The characteristic bands of glycolic acid are observed at 3247 and 1703 cm^{-1} corresponding to OH and C═O stretching vibrations, in agreement with the reported study (Ahokas et al., 2018). The asymmetric and symmetric vibrations of N─H stretching of 4-aminopyridine are assigned to the bands at 3433 and 3301 cm^{-1}, which are in line with reported work (Ramalingam et al., 2010). The N─H in-plane bending vibrations appear at 1646 cm^{-1}, and the out-of-plane bending vibrations are assigned at 989 cm^{-1}. The peaks in the region 1600–1500 cm^{-1} are attributed to the C═N ring stretching vibrations (Ramalingam et al., 2010). The peak at ~1000 cm^{-1} is the ring breathing mode of an unpaired pyridine ring (Hawthorne et al., 2013). The hydrogen bond between the pyridine moiety and glycolic acid leads to the ring breathing vibration frequency blue shift. For the glycolic acid-nicotinamide system, this phenomenon is not apparent. The two nicotinamide main bands are observed at 3354 and 3148 cm^{-1} in the NH_2 stretching vibration region (Garbacz et al., 2020). The C═O stretching vibration of nicotinamide is at 1674 cm^{-1}. Furthermore, the two bands for the eutectic mixture at 3338 and 3202 cm^{-1} can be assigned to the glycolic acid-nicotinamide hydrogen bonding interaction (Cuadra et al., 2016). The results of the other solvent systems were provided in supplementary material (Fig. S2). The viscosities of the widely studied hydrophilic DES were relatively high (as high as 2000 Pa·s at ambient conditions) (Fan et al., 2021b). These pyridine-based eutectic mixtures possessed appropriate viscosities, which ranged from 237.9 to 5320 mPa·s at 298.15 K (Table S1).

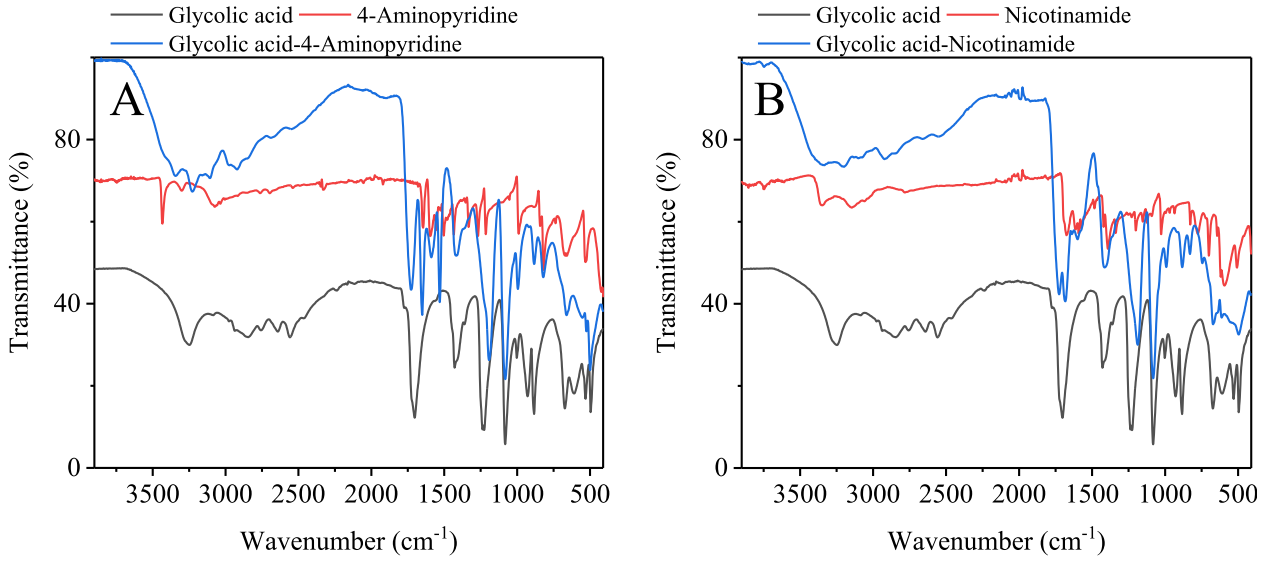

Fig. 3 Fourier transform infrared spectroscopy spectra for deep eutectic solvents and its components. (A) Glycolic acid-4-aminopyridine system; (B) Glycolic acid-nicotinamide system. HBA: HBD (glycolic acid) molar ratio 1:5.

3.2. Liquid–liquid partitioning behaviour

Distribution coefficients and selectivity were employed to evaluate the extraction performance of these eutectic solvents toward perfluorinated iodoalkanes. Four phenolic compound-based DESs with the same HBD were employed for the comparison among groups. Fatty acids with different alkyl chain length were chosen as the disturbing substances because their carbon skeleton and characteristic functional group are similar to that of perfluorinated compounds. Differences in the partition coefficients in terms of the type of HBAs are expected to result in their successful selective extraction. The studied HBAs can be divided into four distinct groups: the pyridine ring, the pyridine ring with the NH_2 group, the pyridine ring with the OH group, and the pyridine ring with the C═O group. As displayed in Fig. 4 (A) and Table S2, the order of the distribution coefficient is, in general, as follows: pyridine ring with C═O group > pyridine ring > pyridine ring with NH_2 group ≈ pyridine ring with OH group ≈ phenolic compounds. In more detail, the values of the distribution coefficient become larger in the order of methyl nicotinate ≈ nicotinic acid < nicotinohydrazide < 2-picolinic acid < nicotinamide. Especially for PFHxI and PFOI, the relatively short-chain targets studied, the extraction efficiencies of DESs with the C═O group are relatively high (0.37–1.80). While their extraction efficiencies toward fatty acids with the same length of carbon chain were in the range of 0.01–0.26. This performance is promising because of the difficulty of short-chain PFASs removal (Wang et al., 2022). For fatty acids (structural analogues), the values of the distribution coefficient become larger in the order of 2-picolinic acid ≈ nicotinamide < methyl nicotinate < nicotinic acid < nicotinohydrazide. Therefore, to consider the distribution coefficient and selectivity together, the glycolic acid-nicotinamide solvent system would be the optimal candidate. The different functional groups of DESs render distinct partitioning behaviours. The inner mechanism can be preliminarily investigated by the quantitative analysis of molecular surface.

3.3. Survey of electrostatic potential surface

The corresponding molecular electrostatic potential maxima for five targets are presented in Fig. 5. A positive "σ-hole" is detected in each perfluorinated iodoalkane. An electronegative "belt" orients in a plane perpendicular to the bond axis, and the maximum (positive) in the molecular electrostatic potential is located over the iodine atom. Their values increase in the following order: PFDeI < PFDoI < PFBI < PFOI < PFHxI. The maxima indicate their relative halogen bond donor abilities. It suggests that these targets should have molecular recognition properties and could therefore form special complexes with relatively strong non-covalent bonding acceptors like pyridines. In addition, as mentioned above, the extraction performances of the DESs toward the relatively short-chain targets were better than those toward long-chain targets. The tendency paralleled the electrostatic potential maxima on the donor halogen atom.

Because halogen and hydrogen bonding interactions are almost electrostatically driven, the molecular electrostatic potential of glycolic acid, pyridines, and perfluorinated iodoalkanes was calculated. Halogen bond is analogical to hydrogen bond in many aspects, and it is comparable to hydrogen bond; thus, competitions may occur between them (Li et al., 2010). As an illustration, electrostatic potential isosurfaces for the starting materials of DESs are shown in Fig. 6. The electrostatic potential surface minima and maxima are represented as the green and yellow spheres. The interaction among HBA, HBD, and target is expected to occur along these minimum/maximum points (Liu et al., 2021). This can be treated using a simple electrostatic model, where the positive electrostatic region on the surface of the iodine-based substance interacts with the negative electrostatic region on the

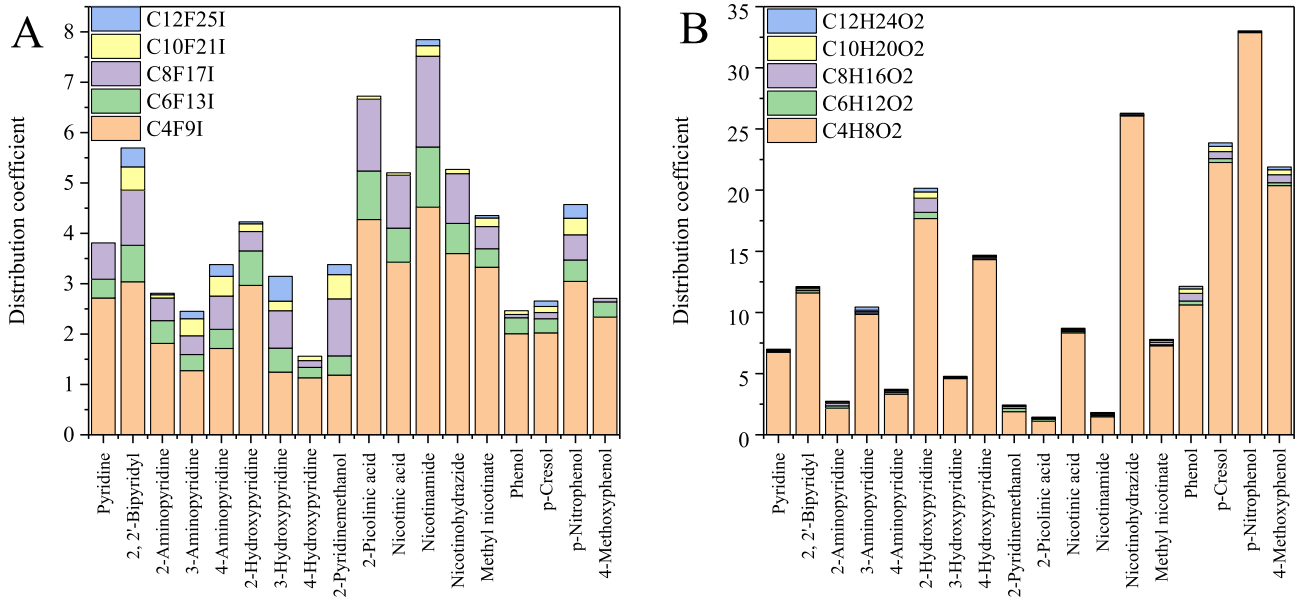

Fig. 4 Experimental liquid–liquid equilibrium results of deep eutectic solvents toward to perfluorinated iodoalkanes (A) and fatty acids (B).

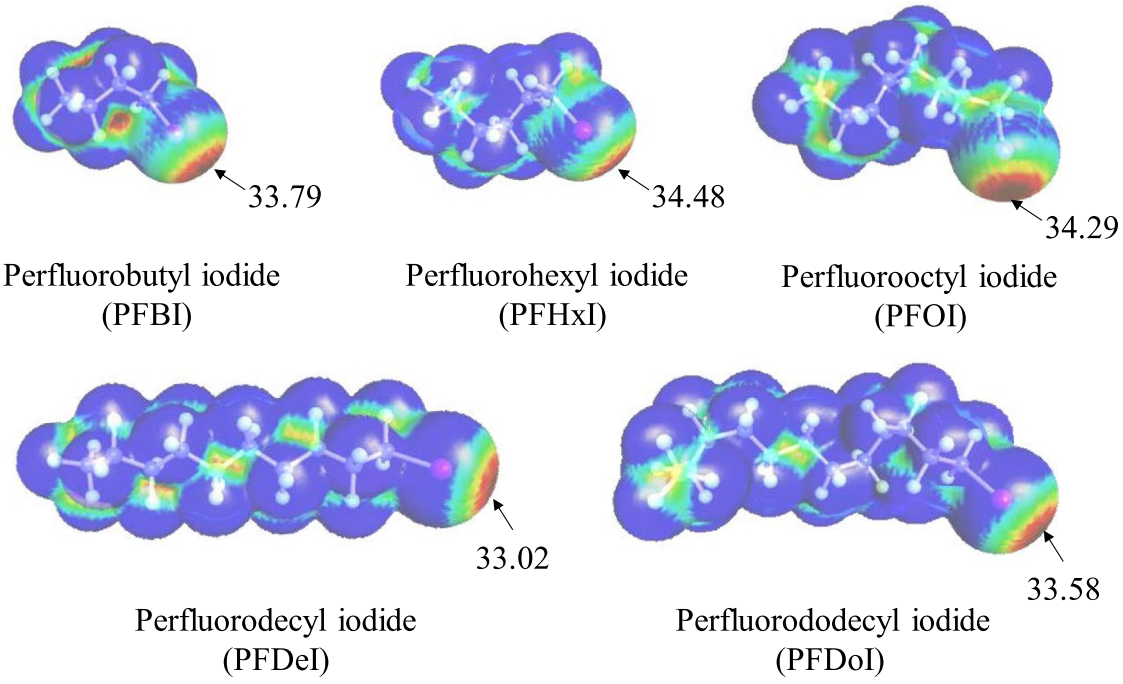

Fig. 5 Electrostatic potential on the 0.001 au molecular surface of perfluorinated iodoalkanes. Numerical labels are represented as red regions corresponding to the global maxima on each surface. Color range (kcal/mol): red, > 20; yellow, between 20 and 10; green, between 10 and 0; blue, negative.

surface of pyridine (Cabot and Hunter, 2009). For pyridine and pyridines with an NH_2 group, the global minimum (the only one) on the surface is located on the nitrogen atom of the pyridine ring. A competition of σ-hole bonding with hydrogen bonding would occur between glycolic acid and perfluorinated iodoalkane, thus leading to a reduction in extraction efficiency. For pyridines with the OH group, the greatest negative electrostatic potential is located over the nitrogen atom of the pyridine ring. The glycolic acid tends to form hydrogen bonds with them during the melting process, and then the target will bind with the second site (OH group). As a consequence, this resulted in lower extraction efficiency and selectivity. For pyridine ring with the C═O group, the most negative potential is localized mostly on the C═O group, thus the above investigations do not excite. Correspondingly, the extraction efficiency drops when the most negative point is replaced by the nitrogen atom of the pyridine ring. The performance of these DESs could be simultaneously affected by their properties such as polarity, acidity, basicity, and so on. Nicotinamide presents a surface that is complementary to perfluorinated iodoalkane. The iodine atom of the target has a positive region surrounded by its negative potential, and the nicotinamide has negative regions surrounded by its positive potential. This indicates that a possible extended cooperative interaction between DES and perfluorinated iodoalkane leads to the further enhancement of their stability (Cabot and Hunter, 2009).

3.4. Parameters

Different descriptors were conducted and calculated for the structure–property-performance relationship, including topological indice, solvatochromic parameters, H_int, H_MF, H_vdW, infinite dilution activity coefficient, total energy, the lowest unoccupied molecular orbital (LUMO) energy, and the highest occupied molecular orbital (HOMO) energy of solvent. The corresponding data are presented in Table S3, Table S4, and Table S5. The connectivity index was chosen, because it was considered suitable for measuring the extent of branching of the carbon-atom skeleton (Ma et al., 2018). The total energy, LUMO energy, and HOMO energy are important points to evaluate the molecular electrical transport properties, which indicate the chemical robustness of a system (Fan et al., 2019). In general, the obtained solvent systems were stable. Three Kamlet-Taft parameters were studied: α, β and π*, which denote hydrogen-bond donating ability (acidity), hydrogen-bond accepting ability (basicity), and polarizability/polarity, respectively (Jessop et al., 2012). The published work confirmed the significant contribution of HBD in DES to Kamlet-Taft parameters. Most of the studies monitored the change in the alkyl chain length of DES components to tailor the DES polarity (Zhang et al., 2021). As shown in Table S4, a slight change in the functional group of HBA can also significantly alter the π* parameter. The glycolic acid-2-pyridinemethanol system is the highest among the obtained DESs, probably because of permanent dipoles and delocalized bonds (Dwamena and Raynie, 2020). It is interesting to note that all the studied solvents are hydrophilic, and their polarity is relatively large, whereas they can recover hydrophobic perfluorinated iodoalkanes. Therefore, a clear understanding of this phenomenon is essential to helping choose the correct solvent for desired industrial purposes. The Kamlet-Taft hydrogen bonding basicity of the prepared DESs is almost larger than the Kamlet-Taft hydrogen bonding

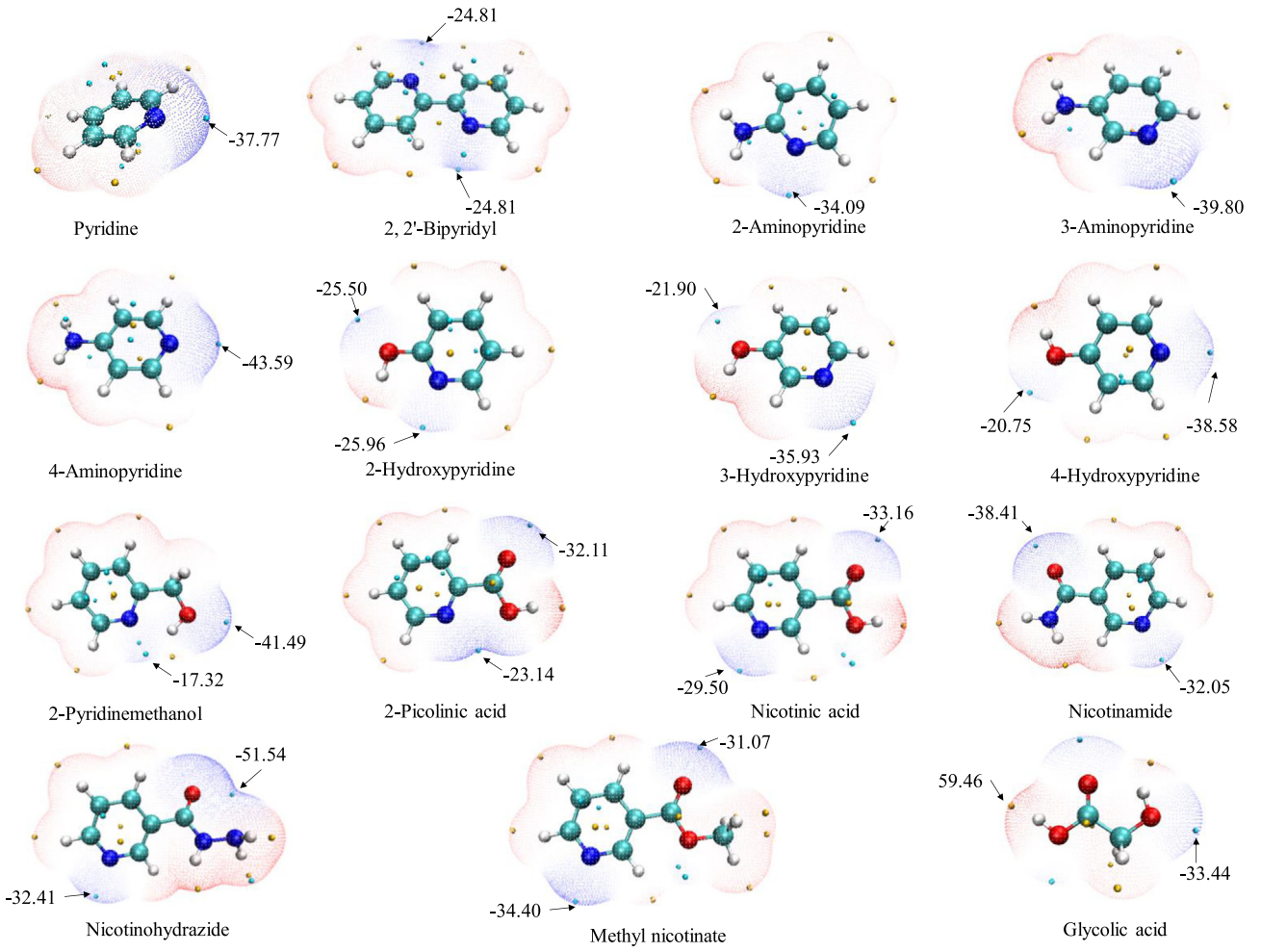

Fig. 6 Electrostatic potential-mapped molecular vdW surface of starting materials corresponding to the ρ = 0.001 au isosurface. The surfaces represent isosurfaces with high electron density regions in blue and low electron density regions in red. The electrostatic potential surface minima and maxima (kcal/mol) are represented as the green and yellow spheres, respectively.

acidity. The highly basic nature of these solvents can be due to the pyridine rings present in the DESs. The activity coefficient predicted by COSMO-RS at infinite dilution is usually utilized to indicate the performance of solvents in liquid–liquid extraction (Dai et al., 2021). The energy data obtained during statistical thermodynamics calculations such as H_int, H_MF, and H_vdW are also useful parameters, which are different from the energy obtained from density functional theory. This model is beneficial in the determination of the general trend rather than the absolute value (Kunov-Kruse et al., 2017).

3.5. Correlation analysis

Differential parameters may be potential factors affecting the extraction performance of DES toward perfluorinated iodoalkane. The correlation among key descriptors, distribution coefficients, and selectivity were analyzed using the Spearman's method (Fig. 7). For the targets with relatively short alkyl chain length (PFBI, PFHxI, PFOI), the results showed that the topological indices of these DESs had a positive correlation with their distribution coefficients, and quantum-chemical parameters of the solvents, including total energy, LUMO energy, and HOMO energy, had a strong negative correlation with their distribution coefficients. For the targets with long alkyl chain length (PFDeI, PFDoI), solvatochromic parameters had a great influence on their distribution coefficients and also on selectivity. Specifically, the π* (polarity) values of these DESs were positively correlated with the distribution coefficients, while α and β were negatively correlated with the distribution coefficients. It is demonstrated that hydrophobic interaction would not play a relatively large role in the extraction of longer-chain targets (Wang et al., 2022). The relevance between the descriptors and the selectivity of the studied DESs is more complicated. Except for PFBI and PFDoI, positive correlations were found between selectivity and topological indices, and parameters obtained with COSMO-RS (H_int, H_MF, H_vdW, activity coefficient). Quantum-chemical parameters also show negative relevance analysis results toward the selectivity of the DESs. Hydrocarbon compounds such as fatty acids are found to be mostly governed by the dispersion force (van der Waals force), whereas the dominant force of perfluoroalkyl chemicals is likely to be

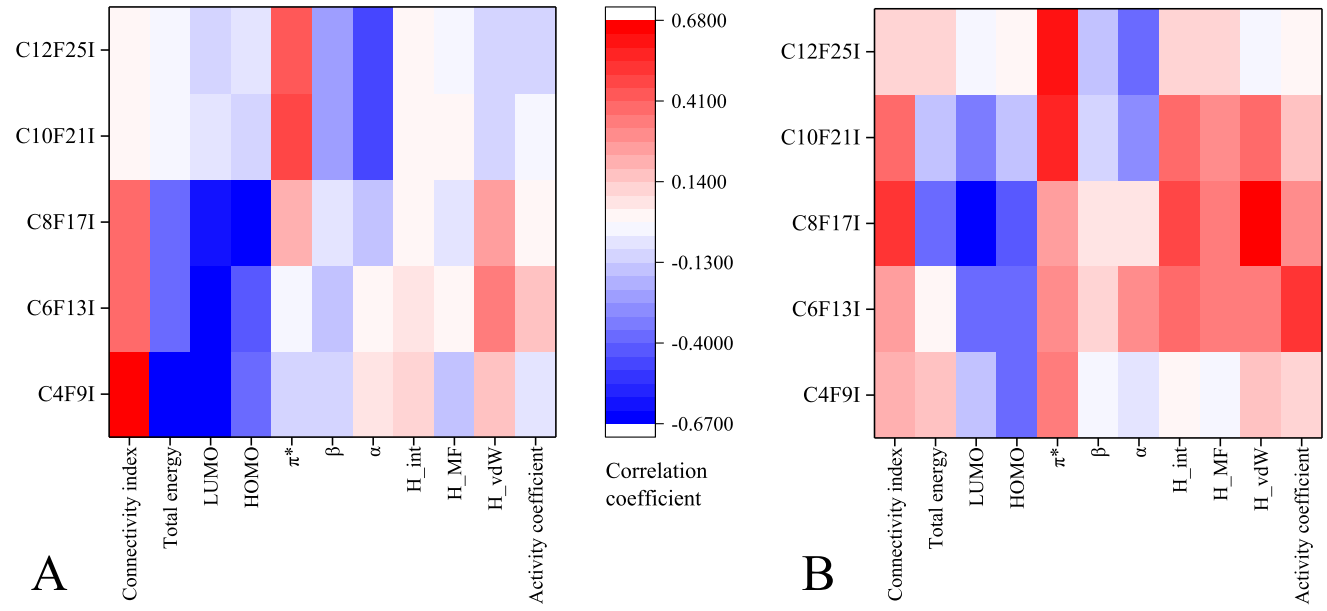

Fig. 7 Correlation coefficient between distribution coefficient and different descriptor (A), between selectivity and different descriptor (B). Red: positive correlation. Blue: negative correlation.

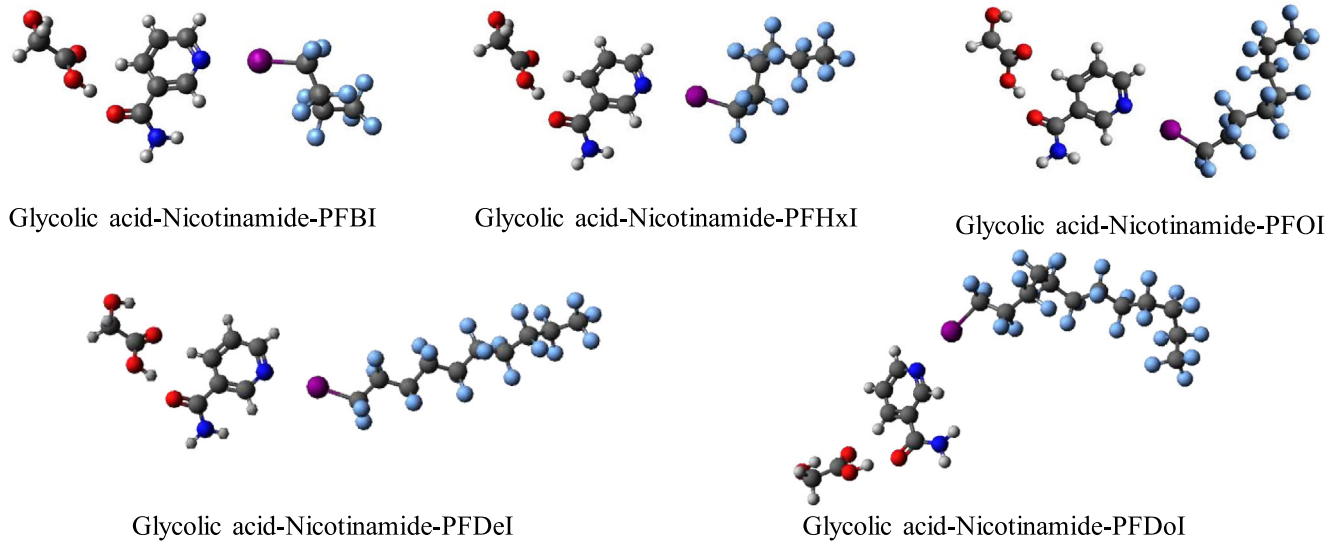

Fig. 8 Optimized geometries of DES-perfluorinated iodoalkane complexes at the M06-2X/aug-cc-pVTZ level.

the dipole–dipole interaction—a kind of orientation force (Hasegawa, 2017).

3.6. Synergism mechanism

As shown in Fig. 8, glycolic acid could form hydrogen-bonded complexes with nicotinamide, and perfluorinated iodoalkane with different alkyl chain length could form halogen-bonded complexes with the DES system. It should be noted that hydrogen bonding interactions and halogen bonding interactions give identical values for the enhancement energy of the ternary complex (Del Bene et al., 2010). In other words, $\Delta\Delta E_{AB} = \Delta E_{AB}' - \Delta E_{AB} = \Delta\Delta E_{BC} = \Delta E_{BC}' - \Delta E_{BC} = \Delta\Delta E$. The relative increasing values of these interactions were defined as $P_{AB} = 100\ \%*\Delta\Delta E/\Delta E_{AB}$, and $P_{BC} = 100\ \%*\Delta\Delta E/\Delta E_{BC}$. The absolute values of $\Delta\Delta E$ become larger in the order of Nicotinamide-Glycolic acid-PFBI < Nicotinamide-Glycolic acid-PFDoI < Nicotinamide-Glycolic acid-PFDeI < Nicotinamide-Glycolic acid-PFOI <. Nicotinamide-Glycolic acid-PFHxI. This is partly consistent with the order of electrostatic potential maxima of perfluorinated iodoalkanes, indicating that halogen bonding interactions play a vital role in these ternary systems. Moreover, there is a good correlation between the halogen-bond strength (ΔE_{BC}, $\Delta E_{BC'}$) and the magnitude of positive electrostatic potential on a halogen atom, supporting the electrostatic interpretation of these halogen bonds (Zhu et al., 2020). It is interesting to note that the relative increment of hydrogen-bond energy is stronger than

Table 2 Interaction energies related parameters (in kcal/mol) [a] at the M06-2X/aug-cc-pVTZ level.

Complex	ΔE_{BC}	ΔE_{AC}	$\Delta E_{AB'}$	$\Delta E_{BC'}$	ΔE_{ABC}	$\Delta\Delta E_{BC}$	P_{AB} (%)	P_{BC} (%)	E_{coop}
Nicotinamide-Glycolic acid-PFBI	−0.2514	−0.1876	−0.5012	−0.2604	−0.7446	−0.0091	5.9141	3.6081	−0.1675
Nicotinamide-Glycolic acid-PFHxI	−0.2661	−0.2059	−0.4992	−0.2796	−0.7495	−0.0136	5.4850	5.1043	−0.1957
Nicotinamide-Glycolic acid-PFOI	−0.2661	−0.2108	−0.4909	−0.2782	−0.7417	−0.0121	4.7428	4.5532	−0.2084
Nicotinamide-Glycolic acid-PFDeI	−0.2545	−0.1886	−0.4894	−0.2652	−0.7288	−0.0107	4.3408	4.2117	−0.1876
Nicotinamide-Glycolic acid-PFDoI	−0.2610	−0.1884	−0.4950	−0.2711	−0.7386	−0.0101	4.6055	3.8702	−0.1839

[a] The various parameters have been defined in the text.

that of halogen-bond energy in all trimer ($P_{AB} > P_{BC}$). It is consistent with the conclusion that the stronger non-covalent interaction has a bigger effect on the weaker one (Saha and Sastry, 2015). E_{coop} is also applied to evaluate the cooperativity of the halogen bonds and hydrogen bonds in their complexes. A negative value of E_{coop} indicates that the two kinds of interactions would work in concert with each other and enhance their strength. Inversely, a positive value reveals that the two interactions show anti-cooperativity (Zhao et al., 2011). From Table 2, it can be clearly seen that the values are negative, which demonstrates the cooperativity effects between the hydrogen and halogen bonds in the ternary complexes regarding the binary complexes. The halogen bonding interaction between nicotinamide and its target is enhanced by introducing hydrogen bonding interaction from glycolic acid. That is to say, the formation of the eutectic system facilitates the extraction of perfluorinated iodoalkanes. The developed solvents can be further utilized in the treatment of perfluorinated iodoalkanes from edible oil, drawing oil, and similar matrixes.

4. Conclusion

Fourteen types of pyridine ring-based DESs containing HBAs with different structures were used to treat perfluorinated iodoalkanes in the oil phase. Results showed that functional groups of HBAs significantly affected the extraction effectiveness of eutectic mixtures. The pyridine ring-based DESs with the C═O group possessed the highest extraction efficiencies among the studied groups. In the end, the glycolic acid-nicotinamide solvent system presented the optimal performance. To some extent, the extraction performances of the DESs paralleled the electrostatic potential maxima on the donor halogen atom and were also substantially affected by the electrostatic potential extrema of pyridine analogues. The correlation study on the structure–property-performance of the DESs showed that the topological indices had a positive relationship with the treatment efficacy of the DESs, and the quantum-chemical parameters of these solvents, including total energy, LUMO energy, and HOMO energy, had a strong negative relationship with them. The solvatochromic parameters of DESs had a great influence on the distribution coefficients and also on the selectivity of these solvents toward targets with long alkyl chain length. Furthermore, the halogen and hydrogen bonds showed cooperativity, which was clarified via quantum-chemistry calculations. The synergism mechanism between them is beneficial to the extraction of perfluorinated iodoalkanes. The utility of developing a proposal for hydrogen-bonding systems in this work will offer the exciting prospect of directionally exploiting and designing multifunctional DESs.

Declaration of Competing Interest

The authors declare that they have no known competing financial interests or personal relationships that could have appeared to influence the work reported in this paper.

Acknowledgement

The authors acknowledge financial support of this work by National Natural Science Foundation of China (32102069).

Appendix A. Supplementary material

Supplementary data to this article can be found online at https://doi.org/10.1016/j.arabjc.2022.104469.

References

Abbott, A.P., Edler, K.J., Page, A.J., 2021. Deep eutectic solvents-the vital link between ionic liquids and ionic solutions. J. Chem. Phys. 155,. https://doi.org/10.1063/5.0072268 150401.

Ahokas, J., Kosendiak, I., Krupa, J., Lundell, J., Wierzejewska, M., 2018. FTIR matrix isolation and theoretical studies of glycolic acid dimers. J. Mol. Struct. 1163, 294–299. https://doi.org/10.1016/j.molstruc.2018.03.019.

Alkorta, I., Elguero, J., Del Bene, J.E., 2010. An ab initio investigation of the properties of H-2:HX hydrogen-bonded complexes. Chem. Phys. Lett. 489, 159–163. https://doi.org/10.1016/j.cplett.2010.02.079.

Balali, M., Sobati, M.A., Gorji, A.E., 2021. QSPR modeling of thiophene distribution between deep eutectic solvent (DES) and hydrocarbon phases: effect of hydrogen bond donor (HBD) structure. J. Mol. Liq. 342,. https://doi.org/10.1016/j.molliq.2021.117496 117496.

Boldrini, C.L., Manfredi, N., Perna, F.M., Capriati, V., Abbotto, A., 2018. Designing eco-sustainable dye-sensitized solar cells by the use of a menthol-based hydrophobic eutectic solvent as an effective electrolyte medium. Chem.-Eur. J. 24 (67), 17656–17659. https://doi.org/10.1002/chem.201803668.

Bryant, S.J., Christofferson, A.J., Greaves, T.L., McConville, C.F., Bryant, G., Elbourne, A., 2022. Bulk and interfacial nanostructure and properties in deep eutectic solvents: current perspectives and future directions. J. Colloid Interface Sci. 608, 2430–2454. https://doi.org/10.1016/j.jcis.2021.10.163.

Cabot, R., Hunter, C.A., 2009. Non-covalent interactions between iodo-perfluorocarbons and hydrogen bond acceptors. Chem. Commun. 2005. https://doi.org/10.1039/b822284c.

Carlson, L.M., Angrish, M., Shirke, A.V., Radke, E.G., Schulz, B., Kraft, A., Judson, R., Patlewicz, G., Blain, R., Lin, C., Vetter, N., Lemeris, C., Hartman, P., Hubbard, H., Arzuaga, X., Davis, A., Dishaw, L.V., Druwe, I.L., Hollinger, H., Jones, R., Kaiser, J.P., Lizarraga, L., Noyes, P.D., Taylor, M., Shapiro, A.J., Williams, A. J., Thayer, K.A., 2022. Systematic evidence map for over one hundred and fifty per- and polyfluoroalkyl substances (PFAS). Environ. Health Persp. 130. https://doi.org/10.1289/EHP10343.

Cuadra, I.A., Cabañas, A., Cheda, J.A.R., Martínez-Casado, F.J., Pando, C., 2016. Pharmaceutical co-crystals of the anti-inflammatory drug diflunisal and nicotinamide obtained using supercritical CO_2 as an antisolvent. J. CO_2 UTIL. 13, 29–37. https://doi.org/10.1016/j.jcou.2015.11.006.

Dai, C., Qi, Z., Lei, Z., Palomar, J., 2021. COSMO-based models. Green Energy Environ. 6, 309–310. https://doi.org/10.1016/j.gee.2021.05.005.

Del Bene, J.E., Alkorta, I., Elguero, J., 2010. Ab initio study of ternary complexes A···NCH···C with A, C = HCN, HF, HCl, ClF, and LiH: energetics and spin−spin coupling constants across intermolecular bonds. J. Phys. Chem. A 114, 8463–8473. https://doi.org/10.1021/jp105220w.

Dwamena, A.K., Raynie, D.E., 2020. Solvatochromic parameters of deep eutectic solvents: effect of different carboxylic acids as hydrogen bond donor. J. Chem. Eng. Data 65, 640–646. https://doi.org/10.1021/acs.jced.9b00872.

Fan, C., Cao, X., Han, T., Pei, H., Hu, G., Wang, W., Qian, C., 2019. Selective microextraction of polycyclic aromatic hydrocarbons using a hydrophobic deep eutectic solvent composed with an iron oxide-based nanoferrofluid. Microchim. Acta 186, 560. https://doi.org/10.1007/s00604-019-3651-y.

Fan, H., Eliason, J.K., Moliva A., C.D., Olson, J.L., Flancher, S.M., Gealy, M.W., Ulness, D.J., 2009, Halogen bonding in iodoperfluoroalkane/pyridine mixtures. J. Phys. Chem. A 113, 14052-14059. https://doi.org/10.1021/jp9057127

Fan, C., Wen, L., Shan, Y., Shan, Y., Cao, X., 2021a. Why do ammonium salt/phenol-based deep eutectic solvents show low viscosity? Arab. J. Chem. 15,. https://doi.org/10.1016/j.arabjc.2021.103512 103512.

Fan, C., Liu, Y., Sebbah, T., Cao, X., 2021b. A theoretical study on terpene-based natural deep eutectic solvent: relationship between viscosity and hydrogen-bonding interactions. Glob. Chall. 5 (3), 2000103. https://doi.org/10.1002/gch2.202000103.

Fan, C., Liu, Y., Shan, Y., Cao, X., 2022. A priori design of new natural deep eutectic solvent for lutein recovery from microalgae. Food Chem. 376,. https://doi.org/10.1016/j.foodchem.2021.131930 131930.

Florindo, C., Branco, L.C., Marrucho, I.M., 2017. Development of hydrophobic deep eutectic solvents for extraction of pesticides from aqueous environments. Fluid Phase Equilibr. 448, 135–142. https://doi.org/10.1016/j.fluid.2017.04.002.

Gaines, L.G.T., 2022. Historical and current usage of per- and polyfluoroalkyl substances (PFAS): a literature review. Am. J. Ind. Med. https://doi.org/10.1002/ajim.23362.

Garbacz, P., Paukszta, D., Sikorski, A., Wesolowski, M., 2020. Structural characterization of co-crystals of chlordiazepoxide with p-aminobenzoic acid and lorazepam with nicotinamide by DSC, X-ray diffraction, FTIR and raman spectroscopy. Pharmaceutics 12, 648. https://doi.org/10.3390/pharmaceutics12070648.

Glüge, J., Scheringer, M., Cousins, I.T., DeWitt, J.C., Goldenman, G., Herzke, D., Lohmann, R., Ng, C.A., Trier, X., Wang, Z., 2020. An overview of the uses of per- and polyfluoroalkyl substances (PFAS). Environ. Sci.-Proc. Imp. 22, 2345–2373. https://doi.org/10.1039/D0EM00291G.

Grabda, M., Zawadzki, M., Oleszek, S., Matsumoto, M., Królikowski, M., Tahara, Y., 2022. Removal of perfluorooctanoic acid from water using a hydrophobic ionic liquid selected using the conductor-like screening model for realistic solvents. Environ. Sci. Technol. 56, 6445–6454. https://doi.org/10.1021/acs.est.1c08537.

Gutiérrez, A., Zamora, L., Benito, C., Atilhan, M., Aparicio, S., 2022. Insights on novel type V deep eutectic solvents based on levulinic acid. J. Chem. Phys. 156 (9), 94504. https://doi.org/10.1063/5.0080470.

Hasegawa, T., 2017. Physicochemical nature of perfluoroalkyl compounds induced by fluorine. Chem. Rec. 17, 903–917. https://doi.org/10.1002/tcr.201700018.

Hawthorne, B., Fan-Hagenstein, H., Wood, E., Smith, J., Hanks, T., 2013. Study of the halogen bonding between pyridine and perfluoroalkyl iodide in solution phase using the combination of FTIR and19 F NMR. Int. J. Spectrosc. 2013, 1–10. https://doi.org/10.1155/2013/216518.

Jessop, P.G., Jessop, D.A., Fu, D., Phan, L., 2012. Solvatochromic parameters for solvents of interest in green chemistry. Green Chem. 14, 1245–1259. https://doi.org/10.1039/c2gc16670d.

Kundu, D., Rao, P.S., Banerjee, T., 2020. First-principles prediction of Kamlet-Taft solvatochromic parameters of deep eutectic solvent using the COSMO-RS model. Ind. Eng. Chem. Res. 59, 11329–11339. https://doi.org/10.1021/acs.iecr.0c00574.

Kunov-Kruse, A.J., Weber, C.C., Rogers, R.D., Myerson, A.S., 2017. The a priori design and selection of ionic liquids as solvents for active pharmaceutical ingredients. Chem. - Eur. J. 23, 5498–5508. https://doi.org/10.1002/chem.201605704.

Lee, J., Jung, D., Park, K., 2019. Hydrophobic deep eutectic solvents for the extraction of organic and inorganic analytes from aqueous environments. TrAC-trend Anal. Chem. 118, 853–868. https://doi.org/10.1016/j.trac.2019.07.008.

Li, Q., Xu, X., Liu, T., Jing, B., Li, W., Cheng, J., Gong, B., Sun, J., 2010. Competition between hydrogen bond and halogen bond in complexes of formaldehyde with hypohalous acids. Phys. Chem. Chem. Phys. 12, 6837. https://doi.org/10.1039/b926355a.

Liu, L., Su, B., Wei, Q., Ren, X., 2021. Selective separation of lactic, malic, and tartaric acids based on the hydrophobic deep eutectic solvents of terpenes and amides. Green Chem. 23, 5866–5874. https://doi.org/10.1039/D1GC01088C.

Lu, T., Chen, F.W., 2012. Multiwfn: a multifunctional wavefunction analyzer. J. Comput. Chem. 33 (5), 580–592. https://doi.org/10.1002/jcc.22885.

Ma, Y., Cao, S., Shi, Y., Gutman, I., Dehmer, M., Furtula, B., 2018. From the connectivity index to various Randic-type descriptors. Match-Commun. Math. Co. 80, 85–106.

Makoś, P., Słupek, E., Gębicki, J., 2020. Extractive detoxification of feedstocks for the production of biofuels using new hydrophobic deep eutectic solvents – Experimental and theoretical studies. J. Mol. Liq. 308,. https://doi.org/10.1016/j.molliq.2020.113101 113101.

McDonough, C.A., Li, W., Bischel, H.N., De Silva, A.O., DeWitt, J. C., 2022. Widening the lens on PFASs: direct human exposure to perfluoroalkyl acid precursors (pre-PFAAs). Environ. Sci. Technol. 56, 6004–6013. https://doi.org/10.1021/acs.est.2c00254.

Ramalingam, S., Periandy, S., Mohan, S., 2010. Vibrational spectroscopy (FTIR and FTRaman) investigation using ab initio (HF) and DFT (B3LYP and B3PW91) analysis on the structure of 2-amino pyridine. Spectrochim. Acta A 77, 73–81. https://doi.org/10.1016/j.saa.2010.04.027.

Ruan, T., Wang, Y., Wang, T., Zhang, Q., Ding, L., Liu, J., Wang, C., Qu, G., Jiang, G., 2010. Presence and partitioning behavior of polyfluorinated iodine alkanes in environmental matrices around a fluorochemical manufacturing plant: another possible source for perfluorinated carboxylic acids? Environ. Sci. Technol. 44, 5755–5761.

Saha, S., Sastry, G.N., 2015. Cooperative or anticooperative: how noncovalent interactions influence each other. J. Phys. Chem. B 119, 11121–11135. https://doi.org/10.1021/acs.jpcb.5b03005.

Satlewal, A., Agrawal, R., Bhagia, S., Sangoro, J., Ragauskas, A.J., 2018. Natural deep eutectic solvents for lignocellulosic biomass pretreatment: recent developments, challenges and novel opportunities. Biotechnol. Adv. 36 (8), 2032–2050. https://doi.org/10.1016/j.biotechadv.2018.08.009.

Shishov, A., Makoś-Chełstowska, P., Bulatov, A., Andruch, V., 2022. Deep eutectic solvents or eutectic mixtures? characterization of tetrabutylammonium bromide and nonanoic acid mixtures. J. Phys. Chem. B 126, 3889–3896. https://doi.org/10.1021/acs.jpcb.2c00858.

Taghizadeh, M., Taghizadeh, A., Vatanpour, V., Ganjali, M.R., Saeb, M.R., 2021. Deep eutectic solvents in membrane science and technology: fundamental, preparation, application, and future perspective. Sep. Purif. Technol. 258,. https://doi.org/10.1016/j.seppur.2020.118015 118015.

van den Bruinhorst, A., Kollau, L.J.B.M., Vis, M., Hendrix, M.M.R. M., Meuldijk, J., Tuinier, R., Esteves, A.C.C., 2021. From a eutectic mixture to a deep eutectic system via anion selection: Glutaric acid + tetraethylammonium halides. J. Chem. Phys. 155. https://doi.org/10.1063/5.0050533.

Vasilyev, A., 2014. MathChem: a python package for calculating topological indices. Match-Commun. Math. Co. 71 (3), 657–680. https://doi.org/10.1039/c4ta00158c.

von der Heiden, D., Vanderkooy, A., Erdélyi, M., 2020. Halogen bonding in solution: NMR spectroscopic approaches. Coordin. Chem. Rev. 407,. https://doi.org/10.1016/j.ccr.2019.213147 213147.

Wang, R., Lin, Z., Klemes, M.J., Ateia, M., Trang, B., Wang, J., Ching, C., Helbling, D.E., Dichtel, W.R., 2022. A tunable porous β-cyclodextrin polymer platform to understand and improve anionic PFAS removal. ACS Central Sci. 8, 663–669. https://doi.org/10.1021/acscentsci.2c00478.

Yu, D., Xue, Z., Mu, T., 2022. Deep eutectic solvents as a green toolbox for synthesis. Cell Rep. Phys. Sci. 3, (4). https://doi.org/10.1016/j.xcrp.2022.100809 100809.

Zainal-Abidin, M.H., Hayyan, M., Wong, W.F., 2021. Hydrophobic deep eutectic solvents: current progress and future directions. J. Ind. Eng. Chem. 97, 142–162. https://doi.org/10.1016/j.jiec.2021.03.011.

Zhang, M., Zhang, X., Liu, Y., Wu, K., Zhu, Y., Lu, H., Liang, B., 2021. Insights into the relationships between physicochemical properties, solvent performance, and applications of deep eutectic solvents. Environ. Sci. Pollut. R 28, 35537–35563. https://doi.org/10.1007/s11356-021-14485-2.

Zhao, Q., Feng, D., Hao, J., 2011. The cooperativity between hydrogen and halogen bond in the XY···HNC···XY (X, Y = F, Cl, Br) complexes. J. Mol. Model 17, 2817–2823. https://doi.org/10.1007/s00894-011-0974-y.

Zhu, Z., Xu, Z., Zhu, W., 2020. Interaction nature and computational methods for halogen bonding: a perspective. J. Chem. Inf. Model 60, 2683–2696. https://doi.org/10.1021/acs.jcim.0c00032.

Zubeir, L.F., van Osch, D.J.G.P., Rocha, M.A.A., Banat, F., Kroon, M.C., 2018. Carbon dioxide solubilities in decanoic acid-based hydrophobic deep eutectic solvents. J. Chem. Eng. Data 63 (4), 913–919. https://doi.org/10.1021/acs.jced.7b00534.